Effect of Sr Substitution in $LaMnO_3$(100) on Catalytic Conversion of Acetic Acid to Ketene and Combustion-like Products

*Yafen Zhang, David R. Mullins, and Aditya Savara**

Chemical Science Division, Oak Ridge National Laboratory, Oak Ridge, Tennessee 37831-6201, United States

ABSTRACT

The chemistry of acetic acid reactions was studied over $La_{1-x}Sr_xMnO_3(100)$ surfaces (x = 0, 0.3, or 0.7). Two types of temperature programmed reaction (TPR) experiments were performed: pre-exposure temperature programmed reactions (PE-TPR) as well as continuous-exposure temperature programmed reactions (CE-TPR). The main products observed in both types of experiments were CO, CO_2, H_2O, acetaldehyde, and ketene (ethenone). In acetic acid CE-TPR experiments with 1:1 co-dosing of oxygen, the surfaces showed ketene production in the order of $LaMnO_3(100) > La_{0.7}Sr_{0.3}MnO_3(100) > La_{0.3}Sr_{0.7}MnO_3(100)$. The presence of oxygen increased the relative amount of ketene produced. The results are consistent with ketene being formed by a dehydration mechanism, with that pathway suppressed if there are too many surface oxygen vacancies. The effect of Sr substitution can be explained as increasing the ease of (or initial quantity of) oxygen vacancies, thereby decreasing the amount of surface oxygens which ultimately inhibits both ketene formation and formation of the combustion-like products CO, CO_2, and H_2O. Our interpretation is that both of these routes are catalyzed by sites (or site ensembles) that include surface oxygens, which is consistent with other published studies.

1. Introduction

Reducible metal oxides can catalyze certain types of deoxygenation and dehydration reactions due to their polar surfaces and in some cases due to their ability to store and release oxygen. Consequently, reducible oxides are used in three-way catalysts, water-gas shift catalysts, and even solid oxide fuel cells.[1-2] Additionally, when oxygen vacancies are created, the new sites created can alter the chemistry that transpires.[3-4] At present, deoxygenation reactions of small organic oxygenates is of interest.[5] Some studies have been conducted on powders, but various insights have been gained by studies on single crystal samples, including thin films, using C1 and C2 oxygenates.[3, 6-15]

When acetic acid and other carboxylic acids are used as reactants, there are several principal mechanisms for removal of the oxygen: ketonization, dehydration, and oxygen abstraction.[9, 16-22] Ketonization reactions involve coupling, with the product being acetone when acetic acid is the reactant. Dehydration results in ketene (ethenone), deoxygenation results in acetaldehyde, and subsequent oxygen abstraction (from acetaldehyde) can then result in ethene. Each of the products mentioned have been observed over reducible metal oxides, with surface oxygen vacancies playing a role in the selectivity. For example, surface oxygen vacancies may adsorb certain molecules more strongly than the sites of an oxidized surface, and may remove oxygen from an aldehyde via oxygen abstraction.[6, 23]

In this study, $La_{1-x}Sr_xMnO_3(100)$ perovskite thin films are used to study the reactions which occur in thermal catalytic conversion of acetic acid over these surfaces, to better understand the chemistry that is accessible over perovskite surfaces. Perovskites have the general formula ABO_3. and are generally composed of alkaline, alkaline-earth, or lanthanide cations and transition metal cations. The alkaline or alkaline earth cations occupy the A position, while transition metals such as Ti, Mn, Co, Fe, Ni, and Cr occupy the B position.[24-25] Use of perovskites enables modulation of the redox properties by substitution or doping of the cations.[25-26] This study, involves studying the effect of substituting some La in $LaMnO_3$ with Sr, and is conducted within the larger context of investigating which reactions occur during thermal catalysis of acetic acid reactions over $La_{1-x}Sr_xMnO_3(100)$ surfaces (x = 0, 0.3, or 0.7). This substitution is expected to increase the ease of oxygen vacancy formation,[27] as will be discussed below. In addition to the chemical tunability of perovskites, many perovskites tend to have high thermal stability, high ionic and (in some cases) electron conductivity, which has led to interest in their use for a variety of possible applications.[24, 28-29] Widespread studies of perovskite materials has increased in recent years, though the reactions of small organic molecules over perovskite surfaces is less studied than over binary metal oxides, due to the relatively recent increase in the synthesis of perovskite materials.

In this work, the reaction of acetic acid over three perovskite thin films are studied, $La_{1-x}Sr_xMnO_3(100)$ surfaces ($x = 0$, 0.3, or 0.7). Two types of temperature programmed reaction experiments are used. In the first type of experiment, the surface is pre-exposed to acetic acid (to create adsorbates on the surface) followed by a temperature programmed reaction of the species on the surface.[30] This first type of experiment with preexposure will be labeled PE-TPR. In the second type of experiment, the surface is continuously exposed to acetic acid, with or without co-exposed O_2: a temperature programmed reaction is performed under this continuous exposure, in order to study quasi-steady state catalytic conversion over the surface. This second type of experiment with continuous exposure will be labeled CE-TPR. As will be shown, we find that the selectivities are somewhat different between the PE-TPR and CE-TPR experiments, and the surfaces appear to have continuous activity in the CE-TPR experiments. The results are consistent with ketene being produced through a dehydration mechanism in a way that becomes partially suppressed in the absence of surface oxygen replenishment.

2. Methods

$La_{1-x}Sr_xMnO_3$ thin films were grown on 0.05% Nb-doped $SrTiO_3(100)$ (STO(100)) by pulsed laser deposition (PLD) at the Oak Ridge National Laboratory Center for Nanophase Materials Sciences through a user proposal, following previously established methods.[31-32]. The single crystal substrates were 10 x 10 x 1 mm^2 and non-porous, resulting in ~1 cm^2 of surface area in the final samples. The effects of film roughness will be negligible for order of magnitude estimates of the surface area.[33-34] The films were grown using $La_{1-x}Sr_xMnO_3$ targets of the desired composition with a laser fluence of ~1.5 J cm-2 while the substrate was heated up to 650 °C in a background pressure of 200 mTorr O_2. The film growth was monitored by reflection high-energy electron diffraction (RHEED) that indicates a film thickness of ca. 20 nm. The single-crystalline nature of the LMO(100) film was determined by thin film X-ray diffraction (XRD) and the film thickness was confirmed by the thickness fringes in the high-resolution scans of the (002) diffraction peaks ("Epitaxy" software, Panalytical). An $La_{0.7}Sr_{0.3}MnO_3$(100) (LSMO(100)) thin film of ca. 10 nm in thickness was grown epitaxially on a 0.05% Nb-doped STO(100) using PLD and conditions reported previously.[31-32] Using the same methodology and characterization techniques, $LaMnO_3$(100) and $La_{0.3}Sr_{0.7}MnO_3$ were prepared as thin films grown on 0.05% Nb-doped $SrTiO_3$(100) (STO(100)). The RHEED data indicated film thicknesses of ca. 20 nm.

Experiments were performed in an ultrahigh vacuum apparatus at Oak Ridge National Lab, as described previously.[35] The most pertinent details will be included here. The base pressure of the instrument is typically between 1×10^{-10} and 4×10^{-10} Torr. Films were oxidized under an oxygen flux equivalent to ~1×10^{-7} mbar at ~ 800 K for ~30 minutes between experiments.

The acetic acid was introduced using a cylindrical-tube directed gas doser with a 10 μm diameter aperture.[36] A high sticking coefficient (>0.30 for the zero coverage limit) is expected for acetic acid.[37] For PE-TPR, acetic acid exposure was conducted at 190 K, with the temperature ramp going from 190 K to 800 K at 2 K s^{-1}. During CE-TPR acetic acid exposure was started at 300 K, with the temperature ramp going from 300 K to 800 K at 1 K s^{-1}. Gases evolved were monitored with a Hiden HAL/3F 301 mass spectrometer. The PE-TPR occurred in a "line-of-sight" geometry with the sample facing the ionization region of the mass spectrometer and within several centimeters of it. For CE-TPR, the sample was facing the doser with a small gap between sample and doser (~1-2 mm) with the angle between the sample face and the mass spectrometer ~ 90 degrees, and the temperature ramp was 1K s^{-1}. The general principles used during these CE-TPR experiments are described elsewhere,[38] but will be briefly described here. This geometry during CE-TPR ensures that >90% of the reactants initially collides with the sample, and that <<1% of the reactants have a direct line of site exposure to the mass spectrometer. Molecules that enter the chamber have a much lower chance of re-encountering the sample: a typical CE-TPR experiment has a flux equivalent to ~10^{-6} mbar on the sample, while the molecules that enter the rest of the chamber result in steady state chamber pressures during CE-TPR of ~10^{-8} mbar. This steady state of molecules in the chamber is effectively an 'effluent' flux, and is what the concentrations measured by the mass spectrometer reflect. The molecules in the ultrahigh vacuum chamber environment do not have a direct line of site to the sample face, and result in a flux on the sample that is $\leq$2 orders of magnitude lower than the directed reactant flux on the sample face, and are thus negligible relative to the intentional dosing.

The masses monitored during experiments were subsets of: 2, 14, 16, 18, 26, 27, 28, 29, 31, 32, 42, 43, 44, 45, 58, 60. The signals were baseline corrected. These masses were assigned to the following molecules: 2 (H_2 and other molecules), 14 (ketene), 16 (methane), 18 (H_2O), 26 (ethyne and ethylene), 27 (ethylene), 28 (CO and other molecules), 29 (acetaldehyde, acetic acid), 31 (ethanol), 42 (ketene, acetic acid), 43 (acetic acid), 44 (CO_2 and other molecules), 45 (acetic acid), 58 (acetone), 60 (acetic acid). Reference patterns for the molecules were obtained from the NIST webbook.[39] These resolved signals were then converted to resolved molecular concentrations (arbitrary units, but a common scale) based on correction factors determined using the method of Madix and Ko (an example calculation is provided in the reference cited).[40] The data was then plotted and smoothed to remove noise in OriginPro 2015. As can be observed in the graphs, 'imperfections' in the data were retained by this smoothing, such that even features of much smaller width than the observed peaks were retained.

In both the PE-TPR experiments and the CE-TPR experiments, the H_2O signals are a little less than half what would be expected based on mass balance. The lower H_2O signals are assumed to be from a combination of imperfections in the mass-spectrometry scaling factors, and from H_2O being a more sticky molecule than the other molecules (i.e., H_2O that is generated may stick to various metal surfaces in the chamber and thus result in decreased detected signals). Acetic acid has a long residual lifetime in the chamber due to being a very sticky molecule, and quantitative analysis of the acetic acid signals was not attempted for this reason.

3. Results and Discussion

3.1 PE-TPR with Acetic Acid on $La_xSr_{1-x}MnO_3(100)$

Figure 1 shows the PE-TPR results following acetic acid adsorption on $LaMnO_3(100)$ (LMO), $La_{0.7}Sr_{0.3}MnO_3(100)$, and $La_{0.3}Sr_{0.7}MnO_3(100)$. The traces shown in Figure 1 correspond to attributed gas-phase concentrations based on signals detected in the mass spectrometer. The PE-TPR experiments produced water, CO_2, CO, and ketene, as the major products; accompanied by the formation of some acetaldehyde and H_2. These same products have been observed over $CeO_2(100)$, $CeO_2(111)$, $UO_2(111)$, $TiO_2(100)$, and Fe_3O_4, with the main peaks of the organic products generally observed under similar temperature ranges as in this study (550-750 K).[9, 17, 21, 41-42] For the experiments reported here, evidence of acetone and ethene formation were not observed.

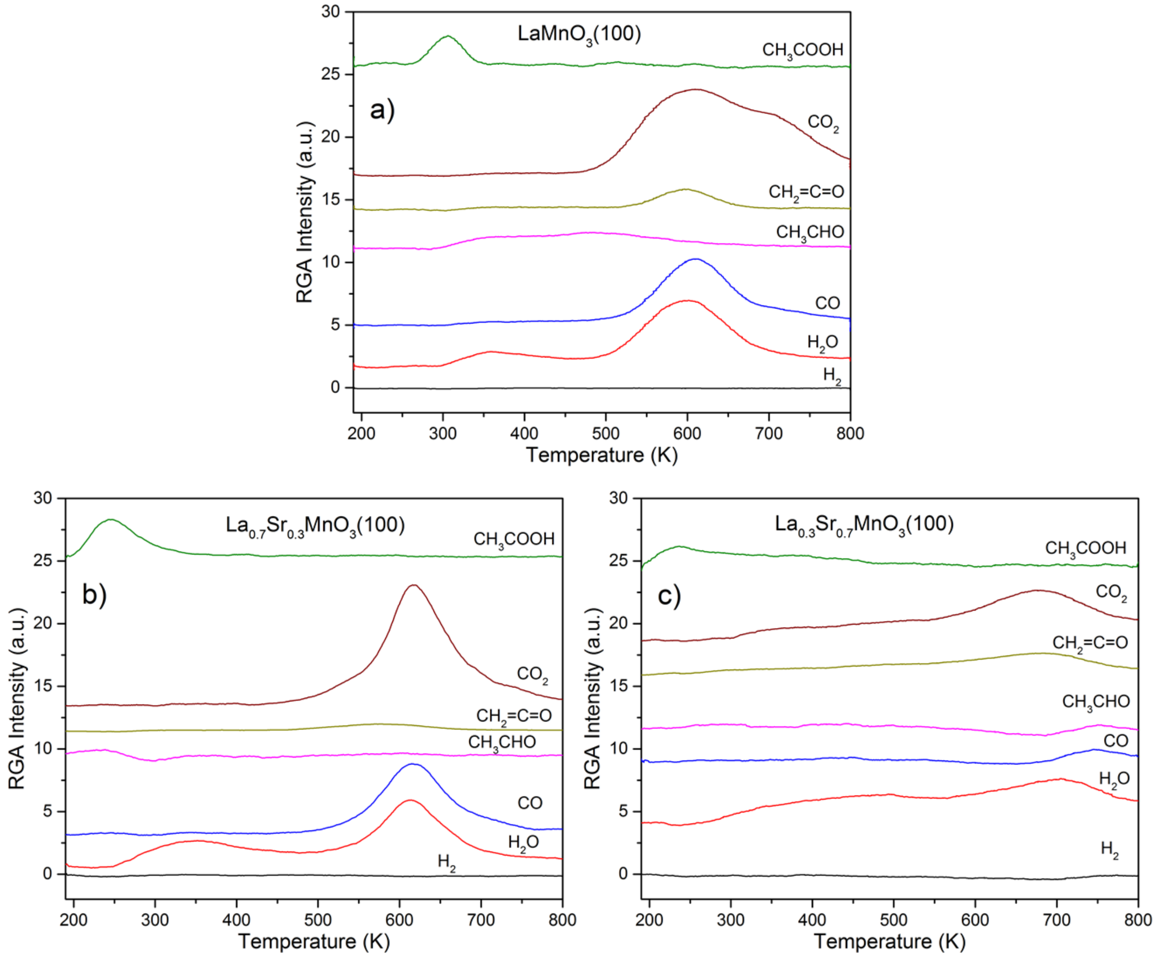

Figure 1. Concentration normalized mass spectrometry signals during PE-TPR following the adsorption of acetic acid at 190 K from $La_{1-x}Sr_xMnO_3(100)$ surfaces with (a) x = 0, (b) x = 0.3, and (c) x = 0.7. The traces for each molecule have been vertically shifted for clarity.

We begin our discussion of these results by considering the peaks observed in Figure 1 and the corresponding temperatures for those peaks. The temperatures of dosing and the subsequent temperature programmed reaction in these experiments were ≥ 190K, and are thus expected to exclude any multilayer adsorption and desorption.[17] Multilayer desorption of acetic acid would be expected to appear at < 190 K, if multilayers are present, and there is no CH_3COOH peak seen at the start of heating in these experiments.[17] The peak attributed to CH_3COOH at ~230-300 K (appearing in Figures 1a through 1c) is less than 0.25 monolayers for each surface, based on carbon balance with the other products observed. The two plausible interpretations of this CH_3COOH

peak are that it arises from the desorption of a weakly adsorbed molecular acetic acid species, or that it arises from recombination of dissociated species (surface monodentate/bidentate acetates and hydrogen).[43] We tentatively ascribe these signals as arising from recombination of surface acetates with surface hydrogens (Equation 1), which is consistent with our next point. As the surface temperature is increased to 300 K, water is produced on each of the surfaces studied. It has been shown that cerium oxide[4, 44-45] and titanium dioxide[46] produce water in similar temperature ranges via lattice oxygens and adsorbed hydrogen that originated from adsorbate dissociation (these hydrogens are commonly referred to as hydroxyls, as the hydrogens are adsorbed on surface oxygens). We therefore attribute the water produced to coming from two adsorbed hydrogens and a lattice oxygen (Equation 2), which is consistent with the interpretation that acetic acid adsorbs on LMO/LSMO dissociatively, as is common on metal oxides:

$$CH_3COOH\ (a) \leftrightarrow CH_3COO\ (a) + H\ (a) \tag{1}$$

$$2\ H\ (a) + O\ (l) \rightarrow H_2O\ (g) + V_O \tag{2}$$

where species marked with (a) are adsorbed species, the O(l) is a lattice oxygen, and the V_O is an oxygen vacancy.

This mechanism for H_2O production would create oxygen vacancies that may further stabilize the adsorbed acetate. The majority surface species that are present on the surface (presumed to be acetates[17]) undergo further reactions at higher temperatures (above 450 K) such as dehydration to form ketene, deoxygenation to form acetaldehyde, and oxidation to form gas-phase CO, CO_2, and H_2O. In various temperature ranges, other minor products such as acetaldehyde are observed. Methane is either not produced or is produced only in very small quantities: as suggested by one of the reviewers, there may be a route where the CH_3 group from some acetates give rise to surface carbon that subsequently becomes oxidized to produce CO_2 (and H_2O).

Very broadly speaking, the TPR spectra can be divided into two temperature regions: some sets of products are observed at < ~450 K while most of the products are observed at > ~450 K. To aid in further discussion, the integrals of the signals of various products are shown in Figure 2 for these two temperature ranges.

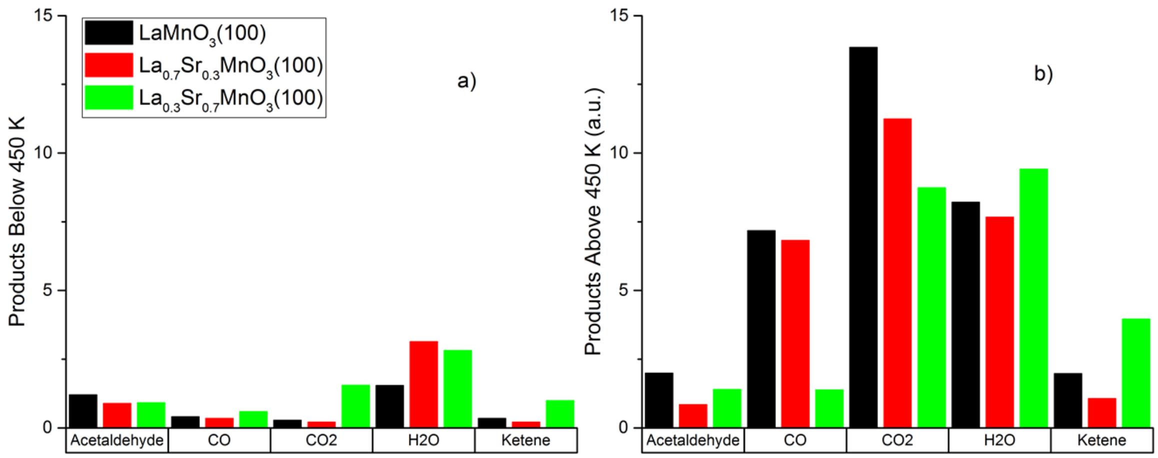

Figure 2. Integrated product distribution from PE-TPR of acetic acid on $LaMnO_3(100)$, $La_{0.7}Sr_{0.3}MnO_3(100)$, and $La_{0.3}Sr_{0.7}MnO_3(100)$ surfaces (a) below 450 K and (b) above 450 K. The bars heights represent the total amount produced, proportional to the number of molecules.

The integrals that have been consolidated in Figure 2 exhibit the product distributions from PE-TPR from acetic acid for the temperature regions below and above 450 K on the three surfaces. Comparison of Fig. 2a with 2b demonstrates that most of the gas phase products are observed above 450 K, with the main low temperature product being the 'low temperature' water production discussed earlier. At >450 K, CO, CO_2, and H_2O become the major products. It is interesting that these products, normally associated with combustion, are the dominant products for acetic acid PE-TPR over each of the surfaces in these experiments. The C:O ratio in acetic acid is the same as in CO, so it would be stoichiometrically possible to produce solely CO and H_2. However, that is not the kinetically favored route: H_2O and CO_2 are observed in addition to CO, which indicates a mechanistic route that is combustion-like (that is, towards nonselective oxidation[47]). Given that there is no gas-phase supply of oxygen, the product distribution suggests that lattice oxygens are involved in the production of the gas phase molecules observed. This implies that oxygen vacancies are also being created at the surface of the catalyst even in the higher temperature region of the PE-TPR, by a combustion-like mechanism, though these vacancies may migrate to the interior. Published reports indicate that reducible oxides are known to perform decarboxylation of carboxylic acids (to produce CO_2) accompanied by H_2O formation and the loss of surface oxygens, consistent with the results reported here.[48] As pointed out by one of the reviewers, there is a possibility that the PE-TPR product distribution could be affected by carbon deposited on the surface. The amount of C deposited by such a pathway would be between 0-2 carbons per C producing acetic acid molecule, given that the most extreme C producing stoichiometry would still be balanced ($CH_3COOH \rightarrow 2C + 2H_2O$). Future studies may help to clarify whether any C is created and then removed before (or remains after) the highest temperatures of these PE-TPR experiments.

During these PE-TPR experiments, there is no opportunity for the molecules to re-adsorb on the surface. This means that the high temperature conversion to CO, CO_2, and H_2O production all occurs within a single “surface residence”, wherein the molecule likely goes through several surface intermediates (potentially each being very short-lived) before producing the gas phase products observed. The observation of CO, CO_2, and H_2O among the major products is consistent with similar experiments over $CeO_2(111)$ and $CeO_2(100)$,[9, 17] though on the cerium oxide surfaces the aldehyde and acetone make a relatively larger component of the product distribution (acetone was not observed during the experiments over $La_{1-x}Sr_xMnO_3(100)$ in the present work). The Sr appears to affect the selectivity observed in PE-TPR. The two Sr containing samples displayed increased low temperature H_2O production during PE-TPR relative to the sample without Sr (by approximately a factor of 2 for production at < 450 K, as can be seen in Figure 2a). The samples containing Sr produced less CO_x containing species at >450 K during PE-TPR: the $La_{0.3}Sr_{0.7}MnO_3$ sample produced ~80% less CO and ~40% less CO_2 relative to the $LaMnO_3$ species. The low temperature enhancement in H_2O production can be explained by Sr facilitating lattice oxygen removal, which is consistent with the literature results, as will be discussed later in the manuscript. There is not a monotonic trend for the higher temperature H_2O production in Figure 2b. However, interpretation of the high temperature H_2O production can be better explained if the mechanism for ketene formation is a dehydration mechanism, as discussed in the next paragraph.

We believe the ketene production is occurring by a dehydration mechanism: that is, that the mechanism from acetic acid to ketene involves loss of atoms without addition of atoms, and that the oxygen in the ketene is one of the oxygens originally in the acetic acid. We first note that it is useful to interpret these results after considering those observed for conversion of acetic acid PE-TPR using $CeO_2(111)$ with various extents of reduction (various amounts of oxygen vacancies).[17] $CeO_2(111)$ and the thin films used in this study are relatively easily reducible oxides, and may have similar chemistry. The $CeO_2(111)$ results showed that greater extent of surface reduction suppressed water formation, suppressed ketene formation, and enabled acetaldehyde production. Electron sputtering of $UO_2(111)$ to create oxygen vacancies also suppressed ketene formation from that surface.[42] The results observed over $CeO_2(111)$ and $UO_2(111)$, that reduction suppresses ketene formation may be counterintuitive to some readers (since it requires removal of oxygen from the acetic acid), but is explained by a dehydration mechanism[17] if "too many" oxygen vacancies suppress the dehydration mechanism to ketene. The currently accepted mechanism for catalytic conversion of acetic acid to ketene over metal oxides does involve a lattice oxygen as the adsorption site of hydrogen in Equation 1,[9, 18, 42, 49-51] with this lattice oxygen site becoming empty again when H_2O is formed and desorbs (the final step in the catalytic cycle for conversion of acetic acid to ketene and water). If we assume that a dehydration mechanism is in fact responsible for ketene, this can explain the high temperature H_2O trend observed in Figure 2b. In this case, there are 2 mechanisms for water production: the ketene mechanism, and the combustion-like mechanism(s). The sample with the greatest amount of Sr, $La_{0.3}Sr_{0.7}MnO_3(100)$ surface shows the greatest ketene production in these PE-TPR experiments, while the other two samples show greater CO and CO_2 production (combustion-like pathway), resulting in similar levels of high temperature water production from each of the three samples. For these experiments, Sr substitution appears to push the reactivity towards the ketene route at the expense of the combustion-like route. We note that this may not be due to making the combustion route harder to access: the observed trend may be due to the nature of the surface intermediates present at those temperatures. Recognizing the possibilities of intermediate depletion, we performed continuous exposure experiments, the results of which are presented in the next section.

3.2 CE-TPR with Acetic Acid on $La_{1-x}Sr_xMnO_3(100)$ with and without CE of O_2

To investigate the reactivity of acetic acid on the three thin-film surfaces in the absence or presence of a continuous supply of O_2, we performed continuous exposure temperature-programmed reaction (CE-TPR) experiments while dosing the reactant gases onto the pre-cleaned $LaMnO_3$, $La_{0.7}Sr_{0.3}MnO_3$, and $La_{0.3}Sr_{0.7}MnO_3$ surfaces. During the CE-TPR experiments, the acetic acid flux was equivalent to ~10^{-6} Torr of gas molecules colliding with the surface and the O_2 flux was set equal to either 0% or 100% of the acid flux through pre-mixing of the gases and co-dosing the gases. CE-TPR differs from PE-TPR due changes in the distributions and total coverage of surface species present during experiment: this results in different product selectivities observed in CE-TPR relative to PE-TPR, including due to surface coverage effects[52-

[53] on the kinetics. The data obtained during the CE-TPR experiments are from a continuous detection of gas phase species that are effectively the effluent of a flow-type experiment. At any point in Figures 3 to 5, the surface is at a quasi-steady state with continuous exposure of reactant and continuous pumping of products and unreacted molecules. The thin films are not expected to act as an endless supply of oxygen, and this is one reason that the CE-TPR experiments with oxygen may have different quasi-steady state selectivities.

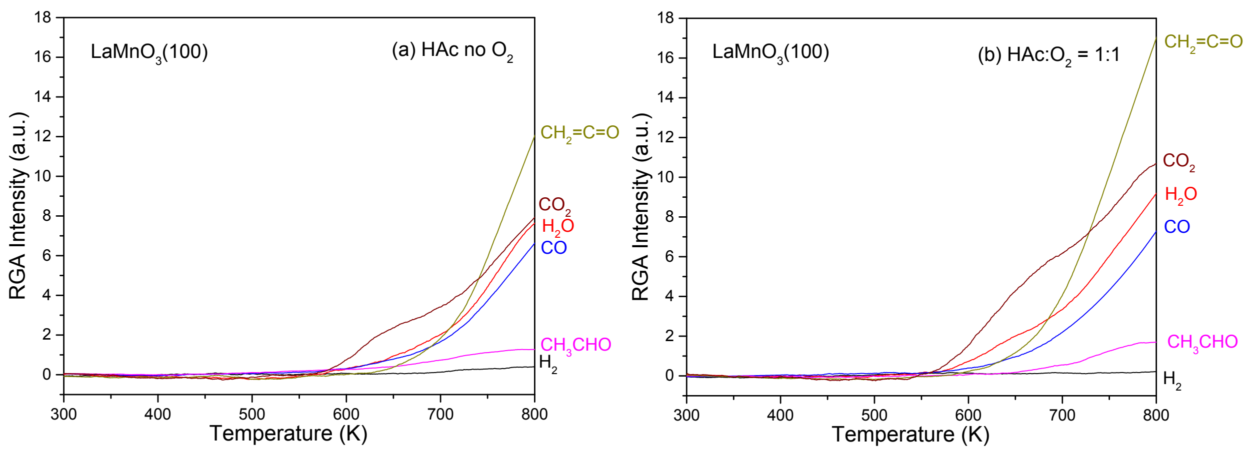

Figure 3. Concentration normalized mass spectrometry signals during CE-TPR of acetic acid on $LaMnO_3(100)$ with the O_2 concentration set equal to (a) 0% or (b) 100% of the acetic acid concentration.

Figure 3 shows the results of CE-TPR when no Sr is substituted into the $LaMnO_3$ perovskite thin film. As shown in Fig. 3a for the case when no O_2 is present, reactions of acetic acid on LMO produce ketene, CO_2, CO, and water as the major products; accompanied with the formation of some acetaldehyde, H_2, and a trace amount of methane (not shown). Evidence of acetone and ethene formation was not observed. With the surface temperature below ~720 K, the gas-phase product is dominated by CO_2. As the temperature increases the dehydration pathway dominates and mostly forms ketene. When O_2 is added the trends are similar, with increased activity. Acetaldehyde is again a minor product both in the absence and presence of O_2. The production of CO_2 dominates the overall reaction at < 700 K, but ketene becomes dominant at higher temperatures.

To investigate the effect of Sr substitution on the acetic acid oxidation, we next performed reaction studies of acetic acid on the $La_{0.7}Sr_{0.3}MnO_3(100)$ surface. As shown in Figure 4, CO_2 is the most abundant product at both low and high temperatures. Outside of the increase CO_2 production, the results are qualitatively similar to those over LMO, with oxygen increasing the quantity of gas phase products, particularly for CO_2 and ketene.

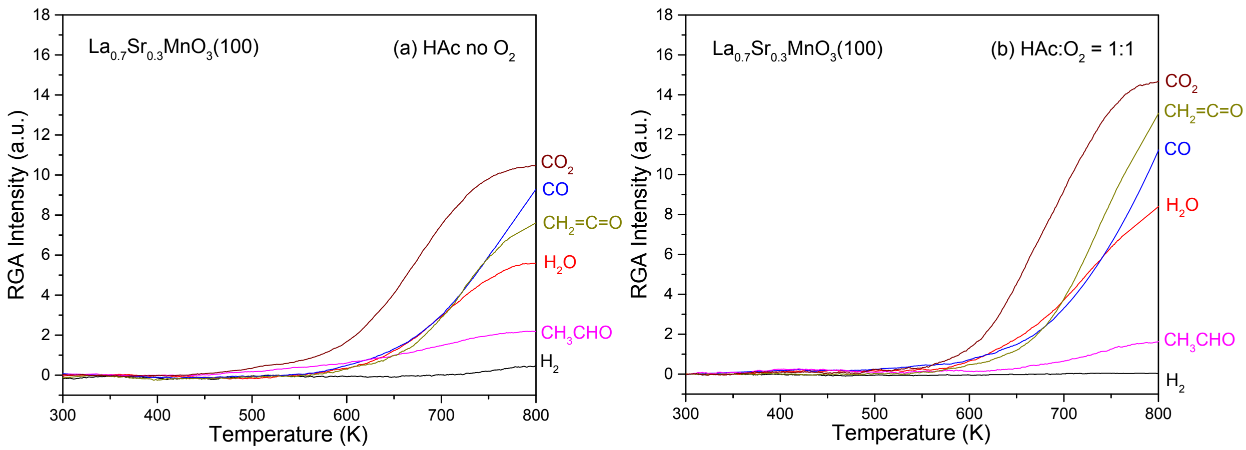

Figure 4. Concentration normalized mass spectrometry signals during CE-TPR of acetic acid on $La_{0.7}Sr_{0.3}MnO_3(100)$ with the O_2 concentration set equal to (a) 0% or (b) 100% of the acetic acid concentration.

Figure 5 shows the results of acetic acid CE-TPR over $La_{0.3}Sr_{0.7}MnO_3$ in the absence and presence of O_2. Unlike what was observed on the other surfaces, the presence of O_2 does not greatly affect the formation of ketene and acetaldehyde, but does appear to hinder the production of H_2, suppresses the trace methane formation and appears to increase the amount of CO_2 formed. As suggested by one of the reviewers, there may be a route where the CH_3 group from some acetates give rise to surface carbon that subsequently becomes oxidized to produce CO_2 (and H_2O).

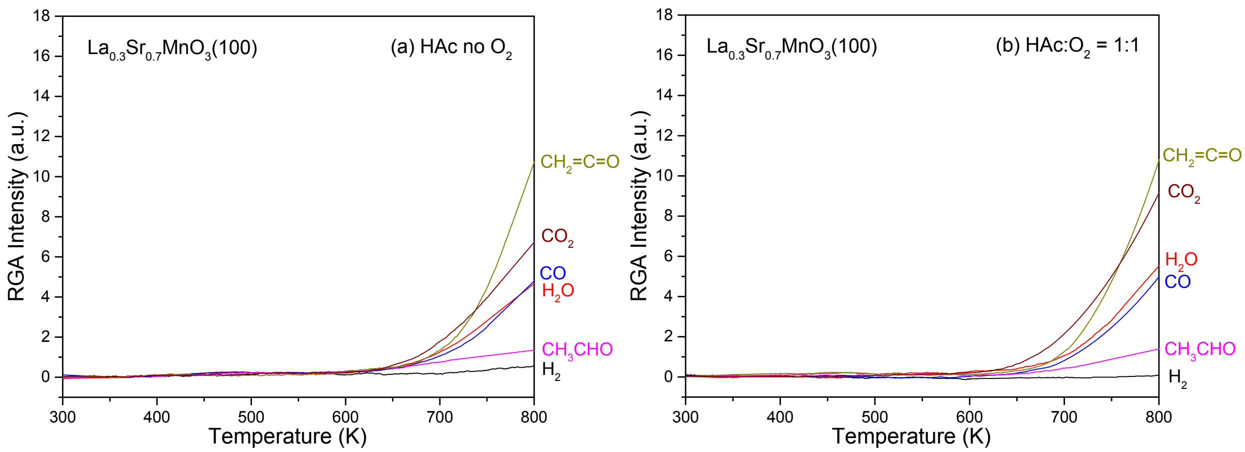

Figure 5. Concentration normalized mass spectrometry signals during CE-TPR of acetic acid on $La_{0.3}Sr_{0.7}MnO_3(100)$ with the O_2 concentration set equal to (a) 0% or (b) 100% of the acetic acid concentration.

The above results can be interpreted as meaning that, in the context of continuous exposures above 750 K, readily available oxygen increases the extent of catalytic reaction while Sr substitution seems to decrease the extent of catalytic reaction – this possibility is explored further below. Figure 6 displays the product distribution during oxidation of acetic acid at 650 K and 800 K with/without O_2 for the 3 surfaces. At 650 K, the less Sr-substituted and non-Sr substituted surfaces are more active in producing CO_2. At a higher surface temperature, all three surfaces become much more reactive towards the major products of CO_2, CO, H_2O, and ketene. The most substituted surface, $La_{0.3}Sr_{0.7}MnO_3$, has the least effect from introducing O_2. In conjunction with the other results reported: the weak effect of oxygen could mean that oxygen vacancies are not created, on this surface, or it could mean Sr increases the ability for the surface to receive oxygen from the bulk so rapidly that gas phase oxygen is not required. Such an interpretation is also consistent with the previously noted conjecture (section 3.1) that O_2's role in promoting ketene production is to fill surface oxygen vacancies, thereby preventing the formation of "too many" surface oxygen vacancies (though one would expect that filling vacancies would also promote the combustion-like route, as will be discussed further). It is clear from comparing Figure 6b and Figure 6d that increased oxygen results in increased products, including ketene (this will be explored further below). Looking across all four panels in Figure 6, the trends with Sr substitution are not strictly monotonic: in some cases 0% substitution has the highest activity, while in other cases the 30% substitution has the highest activity. However, in most cases in Figure 6 the highest Sr substitution has the lowest activity. In particular, the ketene formation at 800 K with oxygen co-dosing shows a clear trend of decreased ketene formation when more Sr is present (Figure 6d). We explore the trends from Sr substitution further in the next figure and paragraph.

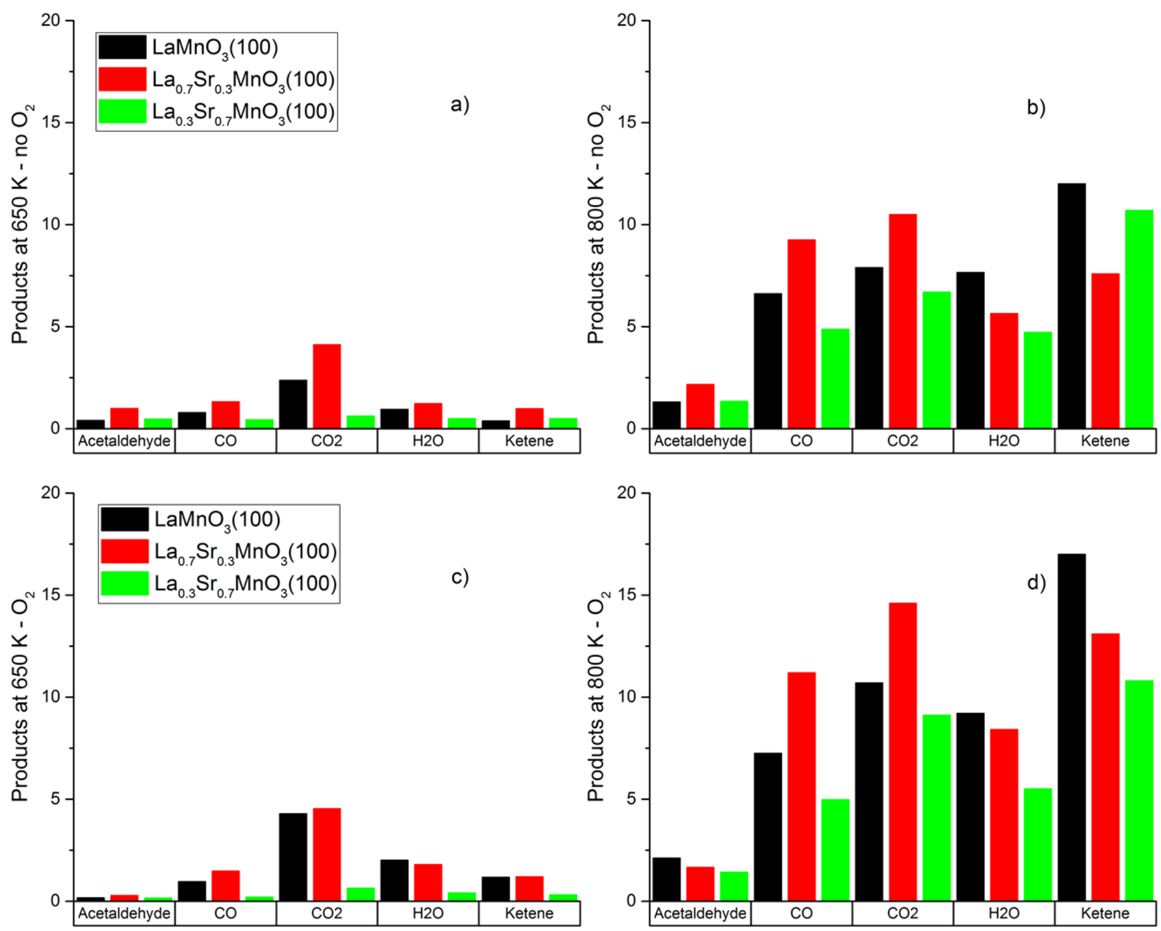

Figure 6. Product distribution from CE-TPR of acetic acid over $LaMnO_3(100)$, $La_{0.7}Sr_{0.3}MnO_3(100)$, and $La_{0.3}Sr_{0.7}MnO_3(100)$ surfaces with the O_2 concentration set equal to 0% or 100% of the acetic acid concentration. Panels on top show the results with no oxygen, panels on bottom show the results with oxygen. The panels on left show the production at the lower temperature chosen of 650 K, while the panels on bottom show the production at the higher temperature chosen of 800 K. The bars heights represent the scaled quasi-steady state amount of product, proportional to the number of molecules.

Figure 7 plots trends for product formation as a function of Sr substitution during CE-TPR at 650 K and 800 K with and without O_2. Figure 7a shows the absolute production of carbon containing products, $C_x(H_y)(O_z)$ taken as the sum of the absolute carbon products scaled by the number of carbons (that is, by a factor of 2 for acetaldehyde, a factor of 2 for ketene, a factor of 1 for CO, and a factor of 1for CO_2). The reactant, acetic acid, is not regarded as a product in CE-TPR, and is therefore excluded from the sums in Figure 7a. Figure 7b shows the absolute production of ketene (no factor of 2). Figure 7c shows the ketene selectivity based on the quantity of ketene produced divided by the factor in 7a (the factor is included in the numerator, as this is based on the selectivity per Carbon atom). We see multiple trends. A) Sr decreases the total amount of conversion of acetic acid to other carbon containing species, with the exception of one data point (Figure 7a). B) There is more ketene production at 800 K than at 650 K: Figure 7b shows that the absolute production of ketene is an order of magnitude higher, and Figure 7c shows that the selectivity towards ketene is roughly doubled. C) There is more ketene production with oxygen than without oxygen (Figure 7b). D) When oxygen is present, the Sr substituted samples have a decreased ketene production relative to the non-substituted sample: the most Sr substituted sample studied (70% substitution) showed approximately 30% less ketene production than the non-substituted sample. This decrease in ketene as a function of Sr substitution is not primarily due to a change in selectivity: the ketene selectivity changes only on the order of 10% with Sr substitution, as shown in Figure 7c. Therefore, the decrease in ketene with Sr substitution is primarily due to the general decrease in activity with Sr substitution (Figure 7a).

The data are consistent with the following interpretation: Sr substitution may make surface oxygen vacancy formation easier and/or occur in greater quantities, and this may decrease both the ketene and combustion-like routes (the former due to the type of surface intermediate needed, and the latter due to needing surface oxygen). Literature reports indicate that Sr substitution into $LaMnO_3$ to make $La_{1-x}Sr_xMnO_3$(100) does not directly introduce oxygen vacancies but makes oxygen vacancy formation more thermodynamically favored,[54-58] and may also favor the vacancies 'segregating' towards the surface.[54] Similarly, previous results show that introducing Sr into $La_{1-x}Sr_xCoO_3$ enhanced the oxygen exchange kinetics.[27] There is some evidence that Sr segregation to/near the surface plays a role in these types of Sr substituted perovskite systems.[54, 59] If Sr makes vacancy formation easier, this explains the increased low temperature H_2O observed during PE-TPR, Figure 2a. During CE-TPR experiments, the Sr could similarly thus cause a higher steady-state of oxygen vacancies which would reduce the activity towards both the combustion-like route and the ketene route (since both require lattice oxygen sites). However, we note that there is at least one exception in the data to the expected behavior from this interpretation: in Figure 6, the 30% Sr substitution case seems to have more combustion-like activity than the 0% substitution case, indicating that the activity and selectivity must have additional factors involved that are not accounted for in this simplistic interpretation. The fact that the selectivity does not change dramatically in Figure 7c suggests that the role of Sr is not to alter the transition state in ketene formation: this is consistent with the interpretation of the primary effect from Sr substitution being to ease the creation of and/or quantity of oxygen vacancy formation. Sr substitution is predicted to facilitate vacancy formation not only for $LaMnO_3$, but also other related perovskites,[56, 58, 60] and these observations about the effects of Sr substitution on catalyzed acetic acid reactions may thus be predictive of the effects of Sr substitution over related perovskites.

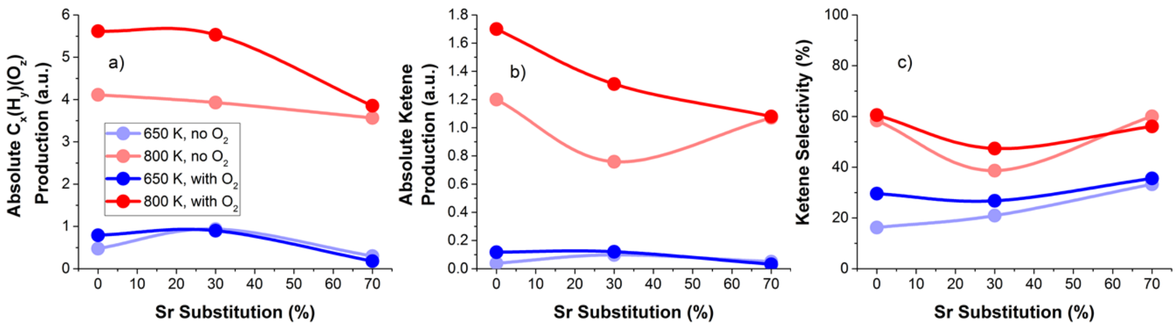

Figure 7. Trends observed in production as a function of Sr substitution during CE-TPR. Lighter symbols without co-dosing of oxygen, darker symbols with co-dosing of oxygen. Blue symbols 650 K, red symbols 800 K. The vertical axis is absolute production or selectivity based on signals proportional to the number of molecules, calculated as described in the text.

3.3 Selectivity Towards Ketene Rather than Possible Products Not Observed

In the present study's experiments, evidence of acetone formation was not observed. Given the elements in the materials studied here, and given that this study investigated single collision events, we will devote a paragraph to compare the results here to those obtained over other metal oxide surfaces. Acetone formation from thermal catalysis of acetic acid has been observed over various metal oxide powders, including La_2O_3, CeO_2, Pr_6O_{11}, Nd_2O_3, Eu_2O_3.[61-63] Multiple mechanisms have been proposed for the ketonization of carboxylic acids over oxides.[20, 61, 63-65] The main possibilities for mechanisms include either a pair of acetates reacting with each other[66] versus a mechanism in which one of the reactants goes through a ketene-like intermediate[63, 65, 67]. It is conceivable that in the powder experiments that ketene could re-adsorb, such that gas phase molecular ketene would be an intermediate towards acetone. However, CeO_2 and TiO_2 surface science experiments observe acetone even without readsorption,[9, 17-18, 21] suggesting that the lack of acetone observed over LSMO(100) and LMO(100) is due to genuine selectivity differences relative to other oxides rather than due to the lack of re-adsorption. Additionally, Martinez et. al. conducted experiments with varying contact times over TiO_2, where it was seen that the selectivity did not change towards acetone with contact time, indicating that (at least the major pathway towards acetone) is not via ketene re-adsorption.[68] Literature publications reported evidence that the deoxygenation to produce acetaldehyde occurs by a Mars van Krevelen oxygen vacancy mechanism,[21, 69-70] and that the ketene and ketone production occur by a different pathway. The literature results are thus in agreement with the present study's results under the following interpretation: the ketene producing mechanism occurs with the participation of at least one non-reduced site, and the lack of acetone in this study is not due to lack of re-adsorption of ketene. Based on the literature reports on cerium oxide and titanium dioxide, there appear to be distinct kinetic pathways to ketene and acetone formation (though these may share a common ketene-like intermediate).[71] There is evidence that the number of coordination vacancies of the cations at the surface is involved in determining selectivity: that multiple coordination vacancies per cation leads to ketonization, and that single coordination vacancies per cation leads to ketene.[47-48, 72] Another factor which has been used to successfully correlate the selectivity towards ketene is the Madelung potential, as experienced by the metal cations and the oxygen ions in the oxide lattice.[42] The Madelung potentials experienced by the O and the Mn in $LaMnO_3$ are reported to be ~+22.5 eV and ~-37.5 eV, respectively.[73] Comparison to Table III of Reference [42] suggests that this type of Madelung potential combination is very similar to that of UO_2(111), and should result in a very high selectivity to ketene during PE-TPR, relative to acetaldehyde and acetone. The results of this work are consistent with that prediction, though the high prevalence of the combustion-like mechanism differs from the other oxides in Table III of Reference, [42] indicating that there is at least one other dimension of complexity that needs to be accounted for in addition to the Madelung potential.

Based on the above considerations, the lack of acetone observed in this study is thus attributed to a genuine selectivity difference relative to other oxides, with LMO(100) and

LSMO(100) favoring ketene rather than acetone. Therefore, we anticipate that the same unusually high selectivity towards ketene would be observed over LMO and LSMO powders, where the 100 face is expected to be dominant from thermodynamic considerations. Ketene (ethenone) has been observed in experiments of acetic acid thermal decomposition[74] as well as from catalytic conversion over some catalytic powders at elevated temperatures,[41, 72, 75] and lowering the temperatures of ketene production with high selectivity could be of practical significance.[71-72, 76-78] Ketene is a relatively unstable and reactive molecule,[79-81] and thus relatively short/controlled contact times may be required to for quantitative detailed studies on the formation of ketene formation using catalytic powders.

4. Conclusions

Two types of temperature programmed reactions were performed with acetic acid over $La_xSr_{1-x}MnO_3(100)$ Surfaces (x = 0, 0.3, or 0.7); pre-exposure temperature programmed reactions (PE-TPR) as well as continuous-exposure temperature programmed reactions (CE-TPR). The main products observed in both types of TPR experiments are Acetaldehyde, CO, CO_2, H_2O, and Ketene. The CO, CO_2, and H_2O products dominate in the PE-TPR experiments (when integrated across the whole temperature range of the experiment). Low temperature (< 450 K) water production was observed in PE-TPR experiments: this is consistent with results of other oxides that suggest that hydrogen atoms produced by dissociation of the adsorbate then form water by extraction of a surface lattice oxygen. In the CE-TPR experiments, the combustion-like products (CO, CO_2, and H_2O) dominate at the "lower" temperature range of ~650 K, with ketene production gradually becoming significant as a function of temperature until ketene is one of the main products at 800 K. In CE-TPR experiments, ketene production is enhanced by the presence of oxygen. In the CE-TPR experiments with oxygen present, the surfaces were most active to least active in the order of $LaMnO_3(100) > La_{0.7}Sr_{0.3}MnO_3(100) > La_{0.3}Sr_{0.7}MnO_3(100)$. Sr substitution had a weaker effect on selectivity than activity. The effects of Sr substitution can be explained in both the PE-TPR and CE-TPR experiments by Sr substitution facilitating the formation of surface oxygen vacancies, without as greatly affecting the transition states towards the main reaction pathways. The results are consistent with surface oxygen vacancies suppressing a dehydration ketene formation, due to partial removal of the type of sites where ketene formation is catalyzed.

AUTHOR INFORMATION

Corresponding Author

*savaraa@ornl.gov

SUPPORTING INFORMATION

Thin film characterization images from Atomic Force Microscopy, reflection high-energy electron diffraction (RHEED)and thin film X-ray diffraction are included in the supporting information for $LaMnO_3(100)/SrTiO_3(100)$

ACKNOWLEDGMENT

The authors thank Thomas Zac Ward and Christopher M. Rouleau for aid in the thin film growth. This work was supported by the U.S. Department of Energy, Office of Science, Office of Basic Energy Sciences, Chemical Sciences, Geosciences, and Biosciences Division. A portion of this research, the thin film growth and characterization, was conducted at the Center for Nanophase Materials Sciences, which is sponsored at Oak Ridge National Laboratory by the Scientific User Facilities Division, Office of Basic Energy Sciences, U.S. Department of Energy.

ABBREVIATIONS

PE-TPR, pre-exposure temperature programmed reaction; CE-TPR, continuous-exposure temperature programmed reaction.

REFERENCES

1. Trovarelli, A., *Catalysis by Ceria and Related Materials*. Imperial College Press: 2002.
2. Park, S.; Vohs, J. M.; Gorte, R. J. Direct Oxidation of Hydrocarbons in a Solid-Oxide Fuel Cell. *Nature* **2000,** *404*, 265.
3. Calaza, F. C.; Xu, Y.; Mullins, D. R.; Overbury, S. H. Oxygen Vacancy-Assisted Coupling and Enolization of Acetaldehyde on CeO_2 (111). *J Am Chem Soc* **2012,** *134*, 18034-18045.
4. Sutton, J. E.; Danielson, T.; Beste, A.; Savara, A. Below-Room-Temperature C-H Bond Breaking on an Inexpensive Metal Oxide: Methanol to Formaldehyde on CeO_2 (111). *J Phys Chem Lett* **2017,** *8*, 5810-5814.
5. Serrano-Ruiz, J. C.; Luque, R.; Sepúlveda-Escribano, A. Transformations of Biomass-Derived Platform Molecules: From High Added-Value Chemicals to Fuelsvia Aqueous-Phase Processing. *Chem Soc Rev* **2011,** *40*, 5266-5281.
6. Mullins, D. R. The Surface Chemistry of Cerium Oxide. *Surf Sci Rep* **2015,** *70*, 42-85.
7. Song, X.; Kuhlenbeck, H.; Freund, H.-J. Surface Reactivity of Titania–Vanadia Mixed Oxides under Oxidizing Conditions. *Top Catal* **2018,** *61*, 792-799.
8. Romanyshyn, Y.; Guimond, S.; Göbke, D.; Sturm, J. M.; Kuhlenbeck, H.; Döbler, J.; Ganduglia-Pirovano, M. V.; Sauer, J.; Freund, H.-J. Methanol Adsorption on V_2O_3 (0001). *Top Catal* **2011,** *54*, 669.
9. Stubenrauch, J.; Brosha, E.; Vohs, J. M. Reaction of Carboxylic Acids on CeO_2 (111) and CeO_2 (100). *Catal Today* **1996,** *28*, 431-441.
10. Abbott, H. L.; Uhl, A.; Baron, M.; Lei, Y.; Meyer, R. J.; Stacchiola, D. J.; Bondarchuk, O.; Shaikhutdinov, S.; Freund, H. J. Relating Methanol Oxidation to the Structure of Ceria-Supported Vanadia Monolayer Catalysts. *Journal of Catalysis* **2010,** *272*, 82-91.
11. Barteau, M. A. Organic Reactions at Well-Defined Oxide Surfaces. *Chem Rev* **1996,** *96*, 1413-1430.
12. Wong, G. S.; Kragten, D. D.; Vohs, J. M. The Oxidation of Methanol to Formaldehyde on TiO_2 (110)-Supported Vanadia Films. *J Phys Chem B* **2001,** *105*, 1366-1373.
13. Feng, T.; Vohs, J. M. A TPD Study of the Partial Oxidation of Methanol to Formaldehyde on CeO_2-Supported Vanadium Oxide. *Journal of Catalysis* **2004,** *221*, 619-629.
14. Zhao, C.; Watt, C.; Kent, P. R.; Overbury, S. H.; Mullins, D. R.; Calaza, F. C.; Savara, A.; Xu, Y. Coupling of Acetaldehyde to Crotonaldehyde on CeO_{2}–X(111): Bifunctional Mechanism and Role of Oxygen Vacancies. *J Phys Chem C* **2018**.
15. Vohs, J. M. Site Requirements for the Adsorption and Reaction of Oxygenates on Metal Oxide Surfaces. *Chem Rev* **2013,** *113*, 4136-4163.
16. Gangadharan, A.; Shen, M.; Sooknoi, T.; Resasco, D. E.; Mallinson, R. G. Condensation Reactions of Propanal over Cexzr1−Xo2 Mixed Oxide Catalysts. *Appl Catal A* **2010,** *385*, 80-91.
17. Calaza, F. C.; Chen, T. L.; Mullins, D. R.; Xu, Y.; Overbury, S. H. Reactivity and Reaction Intermediates for Acetic Acid Adsorbed on CeO_2 (111). *Catal Today* **2015,** *253*, 65-76.
18. Kim, K. S.; Barteau, M. A. Pathways for Carboxylic Acid Decomposition on Titania. *Langmuir* **1988,** *4*, 945-953.

19. Ignatchenko, A. V. Density Functional Theory Study of Carboxylic Acids Adsorption and Enolization on Monoclinic Zirconia Surfaces. *J Phys Chem C* **2011,** *115*, 16012-16018.
20. Ignatchenko, A. V.; Kozliak, E. I. Distinguishing Enolic and Carbonyl Components in the Mechanism of Carboxylic Acid Ketonization on Monoclinic Zirconia. *ACS Catal* **2012,** *2*, 1555-1562.
21. Kim, K. S.; Barteau, M. A. Structure and Composition Requirements for Deoxygenation, Dehydration, and Ketonization Reactions of Carboxylic Acids on TiO_2 (001) Single-Crystal Surfaces. *Journal of Catalysis* **1990,** *125*, 353-375.
22. Idriss, H. Surface Reactions of Uranium Oxide Powder, Thin Films and Single Crystals. *Surf Sci Rep* **2010,** *65*, 67-109.
23. Mullins, D. R.; Albrecht, P. M. Acetaldehyde Adsorption and Reaction on CeO_2 (100) Thin Films. *J Phys Chem C* **2013,** *117*, 14692-14700.
24. Peña, M. A.; Fierro, J. L. G. Chemical Structures and Performance of Perovskite Oxides. *Chem. Rev.* **2001,** *101*, 1981-2018.
25. Polo-Garzon, F.; Wu, Z. Acid–Base Catalysis over Perovskites: A Review. *J Mat Chem A* **2018,** *6*, 2877-2894.
26. Zhu, H.; Zhang, P.; Dai, S. Recent Advances of Lanthanum-Based Perovskite Oxides for Catalysis. *ACS Catalysis* **2015,** *5*, 6370-6385.
27. Lee, D.; Lee, Y. L.; Wang, X. R.; Morgan, D.; Shao-Horn, Y. Enhancement of Oxygen Surface Exchange on Epitaxial $La_{0.6}Sr_{0.4}Co_{0.2}Fe_{0.8}O_3$-Delta Thin Films Using Advanced Heterostructured Oxide Interface Engineering. *Mrs Commun* **2016,** *6*, 204-209.
28. Zhu, J.; Li, H.; Zhong, L.; Xiao, P.; Xu, X.; Yang, X.; Zhao, Z.; Li, J. Perovskite Oxides: Preparation, Characterizations, and Applications in Heterogeneous Catalysis. *ACS Catalysis* **2014,** *4*, 2917-2940.
29. Royer, S.; Duprez, D.; Can, F.; Courtois, X.; Batiot-Dupeyrat, C.; Laassiri, S.; Alamdari, H. Perovskites as Substitutes of Noble Metals for Heterogeneous Catalysis: Dream or Reality. *Chem. Rev.* **2014,** *114*, 10292-10368.
30. Savara, A. Simulation and Fitting of Complex Reaction Network Tpr: The Key Is the Objective Function. *Surf Sci* **2016,** *653*, 169-180.
31. Guo, H. W.; Sun, D. L.; Wang, W. B.; Gai, Z.; Kravchenko, I.; Shao, J.; Jiang, L.; Ward, T. Z.; Snijders, P. C.; Yin, L. F.; Shen, J.; Xu, X. S. Growth Diagram of $La_{0.7}Sr_{0.3}MnO_3$ Thin Films Using Pulsed Laser Deposition. *J Appl Phys* **2013,** *113*.
32. Stoerzinger, K. A.; Hong, W. T.; Azimi, G.; Giordano, L.; Lee, Y.-L.; Crumlin, E. J.; Biegalski, M. D.; Bluhm, H.; Varanasi, K. K.; Shao-Horn, Y. Reactivity of Perovskites with Water: Role of Hydroxylation in Wetting and Implications for Oxygen Electrocatalysis. *J Phys Chem C* **2015,** *119*, 18504-18512.
33. Savara, A.; Schmidt, C. M.; Geiger, F. M.; Weitz, E. Adsorption Entropies and Enthalpies and Their Implications for Adsorbate Dynamics. *J Phys Chem C* **2009,** *113*, 2806-2815.
34. Schmidt, C. M.; Savara, A.; Weitz, E.; Geiger, F. M. Enthalpy and Entropy of Acetone Interacting with Degussa P25TiO $_2$ Determined by Chemical Ionization Mass Spectrometry. *J Phys Chem C* **2007,** *111*, 8260-8267.
35. Calaza, F. C.; Xu, Y.; Mullins, D. R.; Overbury, S. H. Oxygen Vacancy-Assisted Coupling and Enolization of Acetaldehyde on Ceo_2(111). *J Am Chem Soc* **2012,** *134*, 18034-18045.

36. Hagans, P. L.; DeKoven, B. M.; Womack, J. L. A Laser Drilled Aperture for Use in an Ultrahigh Vacuum Gas Doser. *J Vac Sci Technol A* **1989,** *7*, 3375-3377.
37. Chong, S. V.; Idriss, H. The Reactions of Carboxylic Acids on Uo2(111) Single Crystal Surfaces. Effect of Gas-Phase Acidity and Surface Defects. *Surf Sci* **2002,** *504*, 145-158.
38. Libuda, J.; Freund, H. J. Molecular Beam Experiments on Model Catalysts. *Surf Sci Rep* **2005,** *57*, 157-298.
39. Stein, S. E., Mass Spectra. In *NIST Chemistry WebBook, NIST Standard Reference Database Number 69*, National Institute of Standards and Technology.
40. Ko, E. I.; Benziger, J. B.; Madix, R. J. Reactions of Methanol on W(100) and W(100)-(5×1)C Surfaces. *J Catal* **1980,** *62*, 264-274.
41. Grootendorst, E. J.; Pestman, R.; Koster, R. M.; Ponec, V. Selective Reduction of Acetic-Acid to Acetaldehyde on Iron-Oxides. *Journal of Catalysis* **1994,** *148*, 261-269.
42. Chong, S. V.; Idriss, H. Reactions of Acetic Acid on UO_2 (111) Single Crystal Surfaces. *J Vac Sci Technol A* **2000,** *18*, 1900-1905.
43. Davis, J. L.; Barteau, M. A. Hydrogen Bonding in Carboxylic Acid Adlayers on Pd(111): Evidence for Catemer Formation. *Langmuir* **1989,** *5*, 1299-1309.
44. Sutton, J. E.; Overbury, S. H.; Beste, A. Coadsorbed Species Explain the Mechanism of Methanol Temperature-Programmed Desorption on Ceo2(111). *J Phys Chem C* **2016,** *120*, 7241-7247.
45. Mullins, D. R.; Senanayake, S. D.; Chen, T. L. Adsorption and Reaction of C1−C3 Alcohols over CeOx(111) Thin Films. *J Phys Chem C* **2010,** *114*, 17112-17119.
46. Kim, K. S.; Barteau, M. A.; Farneth, W. E. Adsorption and Decomposition of Aliphatic-Alcohols on TiO_2. *Langmuir* **1988,** *4*, 533-543.
47. Schulz, K. H.; Cox, D. F. Reaction Pathways of C3 Carboxylates on Copper(1+) Oxide(100): Acrylic and Propionic Acid Decomposition. *J Phys Chem* **1992,** *96*, 7394-7398.
48. Idriss, H.; Barteau, M. A. Active Sites on Oxides: From Single Crystals to Catalysts. *Adv Catal* **2000,** *45*, 261-331.
49. Peng, X. D.; Barteau, M. A. Dehydration of Carboxylic Acids on the MgO(100) Surface. *Catal Lett* **1990,** *7*, 395-402.
50. Vohs, J. M.; Barteau, M. A. Reaction Pathways and Intermediates in the Decomposition of Acetic and Propionic Acids on the Polar Surfaces of Zinc Oxide. *Surf Sci* **1988,** *201*, 481-502.
51. Kohl, D.; Thoren, W.; Schnakenberg, U.; Schüll, G.; Heiland, G. Decomposition of Gaseous Acetic Acid on SnO_2. *J Chem Soc Far Trans* **1991,** *87*, 2647-2653.
52. Boudart, M. Adsorption Assisted Desorption in Catalytic Cycles. *J Mol Cat A* **1999,** *141*, 1-7.
53. Zaera, F. Probing Catalytic Reactions at Surfaces. *Prog Surf Sci* **2001,** *69*, 1-98.
54. Piskunov, S.; Heifets, E.; Jacob, T.; Kotomin, E. A.; Ellis, D. E.; Spohr, E. Electronic Structure and Thermodynamic Stability of $LaMnO_3$ and $La_{1-x}Sr_xMnO_3$ (001) Surfaces: Ab Initio Calculations. *Phys Rev B* **2008,** *78*.
55. Kuo, J. H.; Anderson, H. U.; Sparlin, D. M. Oxidation-Reduction Behavior of Undoped and Sr-Doped $LaMnO_3$ Nonstoichiometry and Defect Structure. *J Solid State Chem* **1989,** *83*, 52-60.
56. Gan, L.-Y.; Akande, S. O.; Schwingenschlögl, U. Anisotropic O Vacancy Formation and Diffusion in $LaMnO_3$. *J Mat Chem A* **2014,** *2*, 19733-19737.
57. Peng, Y.; Si, W.; Li, J.; Crittenden, J.; Hao, J. Experimental and Dft Studies on Sr-Doped $LaMnO_3$ Catalysts for Nox Storage and Reduction. *Cat Sci Tech* **2015,** *5*, 2478-2485.

58. Su, H.-Y.; Sun, K. DFT Study of the Stability of Oxygen Vacancy in Cubic ABO_3Perovskites. *J Mat Sci* **2015,** *50*, 1701-1709.
59. Chen, Y.; Téllez, H.; Burriel, M.; Yang, F.; Tsvetkov, N.; Cai, Z.; McComb, D. W.; Kilner, J. A.; Yildiz, B. Segregated Chemistry and Structure on (001) and (100) Surfaces of $(La_{1-x}Sr_x)$2coo4 Override the Crystal Anisotropy in Oxygen Exchange Kinetics. *Chem Mat* **2015,** *27*, 5436-5450.
60. Mastrikov, Y. A.; Merkle, R.; Kotomin, E. A.; Kuklja, M. M.; Maier, J. Formation and Migration of Oxygen Vacancies in $La_{1-x}Sr_xCo_{1-y}Fe_yO_3-\Delta$ Perovskites: Insight from Ab Initio Calculations and Comparison with $Ba_{1-x}Sr_xCo_{1-y}Fe_yO_3-\Delta$. *Phys Chem Chem Phys* **2013,** *15*, 911-918.
61. Yamada, Y.; Segawa, M.; Sato, F.; Kojima, T.; Sato, S. Catalytic Performance of Rare Earth Oxides in Ketonization of Acetic Acid. *J Mol Cat A* **2011,** *346*, 79-86.
62. Gliński, M.; Kijeński, J.; Jakubowski, A. Ketones from Monocarboxylic Acids: Catalytic Ketonization over Oxide Systems. *Appl Catal A* **1995,** *128*, 209-217.
63. Pham, T. N.; Sooknoi, T.; Crossley, S. P.; Resasco, D. E. Ketonization of Carboxylic Acids: Mechanisms, Catalysts, and Implications for Biomass Conversion. *ACS Catal* **2013,** *3*, 2456-2473.
64. Pacchioni, G. Ketonization of Carboxylic Acids in Biomass Conversion over Tio2 and Zro2 Surfaces: A Dft Perspective. *ACS Catal* **2014,** *4*, 2874-2888.
65. Pham, T. N.; Shi, D.; Resasco, D. E. Reaction Kinetics and Mechanism of Ketonization of Aliphatic Carboxylic Acids with Different Carbon Chain Lengths over Ru/TiO_2 Catalyst. *Journal of Catalysis* **2014,** *314*, 149-158.
66. Renz, M. Ketonization of Carboxylic Acids by Decarboxylation: Mechanism and Scope. *Eur J Org Chem* **2005**, 979-988.
67. Hendren, T. S.; Dooley, K. M. Kinetics of Catalyzed Acid/Acid and Acid/Aldehyde Condensation Reactions to Non-Symmetric Ketones. *Catal Today* **2003,** *85*, 333-351.
68. Martinez, R.; Huff, M. C.; Barteau, M. A. Ketonization of Acetic Acid on Titania-Functionalized Silica Monoliths. *Journal of Catalysis* **2004,** *222*, 404-409.
69. Pestman, R.; Koster, R. M.; Boellaard, E.; van der Kraan, A. M.; Ponec, V. Identification of the Active Sites in the Selective Hydrogenation of Acetic Acid to Acetaldehyde on Iron Oxide Catalysts. *Journal of Catalysis* **1998,** *174*, 142-152.
70. Doornkamp, C.; Ponec, V. The Universal Character of the Mars and Van Krevelen Mechanism. *J Mol Catal a-Chem* **2000,** *162*, 19-32.
71. Ebrahimi, M.; Rios, J. F.; Leung, K. T. Dissociative Adsorption and Thermal Evolution of Acetic Acid on Si(100)2x1: Surface-Mediated Formation of Ketene and Acetaldehyde from Unidentate and Bidentate Acetate Adsorbates. *J Phys Chem C* **2009,** *113*, 281-289.
72. Libby, M. C.; Watson, P. C.; Barteau, M. A. Synthesis of Ketenes with Oxide Catalysts. *Ind Eng Chem Res* **1994,** *33*, 2904-2912.
73. Yang, C.; Grimaud, A. Factors Controlling the Redox Activity of Oxygen in Perovskites: From Theory to Application for Catalytic Reactions. *Catalysts* **2017,** *7*, 149.
74. Hurd, C. D.; Martin, K. E. Ketene from Acetic Acid. *J Am Chem Soc* **1929,** *51*, 3614-3617.
75. Pestman, R.; Vanduijne, A.; Pieterse, J. A. Z.; Ponec, V. The Formation of Ketones and Aldehydes from Carboxylic-Acids, Structure-Activity Relationship for 2 Competitive Reactions. *J Mol Catal a-Chem* **1995,** *103*, 175-180.

76. Yan, H.; Feng, X.; Liu, Y. B.; Yang, C. H.; Shan, H. H. Catalytic Cracking of Acetic Acid and Its Ketene Intermediate over Hzsm-5 Catalyst: A Density Functional Theory Study. *Mol Catal* **2017,** *437*, 11-17.
77. Padmanabhan, N.; Deshpande, P. K.; Kuloor, N. R. Catalytic Cracking of Acetic Acid to Acetic Anhydride. *Ind Eng Chem Proc Dd* **1968,** *7*, 511-516.
78. Watson, P.; Libby, M.; Barteau, M. Catalyst and Process for Synthesis of Ketenes from Carboxylic Acids. US Patent 05475144, 1995.
79. Guenther, W. B.; Walters, W. D. The Thermal Decomposition of Ketene. *J Am Chem Soc* **1959,** *81*, 1310-1315.
80. Hurd, C. D.; Tallyn, W. H. Optimum Conditions for the Preparation of Ketene from Acetone. *J Am Chem Soc* **1925,** *47*, 1427-1430.
81. Ross, W. F.; Kistiakowsky, G. B. The Photochemical Decomposition of Ketene. *J Am Chem Soc* **1934,** *56*, 1112-1115.

TOC Graphic:

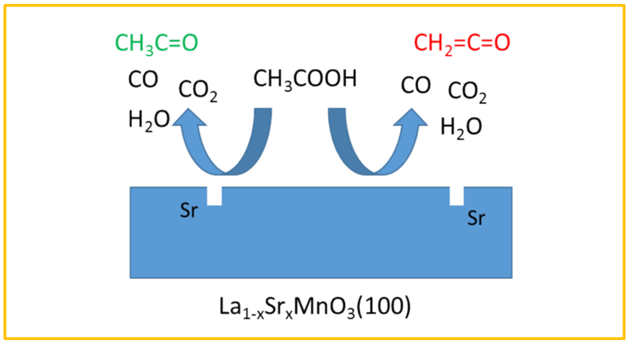

$CH_3C{=}O$
CO
CO_2
H_2O
CH_3COOH
$CH_2{=}C{=}O$
CO
CO_2
H_2O
Sr
Sr
$La_{1-x}Sr_xMnO_3(100)$